Aerial Sensor Networks for Early Wildfire Detection

André Miguel Martins Rocha
andrerocha1998@tecnico.ulisboa.pt

Instituto Superior Técnico, Lisboa, Portugal

October 2021

Abstract

This thesis aims to design an Aerial Sensor Network composed of fixed-wing unmanned aircraft in order to perform surveillance and detect early signs of a wildfire in a given territory. In this work, an algorithm is adapted to uniformly cover a given area and distribute the vehicles in the network depending on the fire hazard risk over the domain to be covered, prioritizing areas with a higher risk. This algorithm is scalable to any number of aircraft and can use any kind of fire hazard risk map that only contains bounded, positive values. Two different dynamical models associated with the movement of fixed-wing UAVs are proposed and are implemented with simulations in Simulink, as well as a ROS implementation to simulate an environment closer to a real world application. Lastly, a probabilistic model is formulated in order to design a workflow to help with the sizing of the fleet and the flight altitude to maximize the probability of detection of wildfires, both via the singular UAVs and the full sensor network.

Keywords: Unmanned Aerial Vehicles, Cooperative Control, Autonomous Surveillance

1. Motivation

During 2017, the burnt area in Portugal saw a 428% increase relative to its mean values, as reported in [7]. In particular, the wildfire of Pedrógão Grande resulted in a burnt area of nearly 45.039 acres [7], causing nearly 500 million euros of estimated damage to the Portuguese government [22]. In fact, Portugal holds the largest percentage of burned area in Europe and is also the country in Europe with the highest number of ignitions per 1000 inhabitants.

While the cause of the previously mentioned fire was unrelated to human activity, the rural fire activity in Portugal is very often caused by humans. Between the years of 2011 and 2021, 48% of the fires with known causes were caused by inappropriate use of controlled fire as reported by Instituto da Conservação da Natureza e das Florestas in [8]. More specifically, 31% are caused by controlled burns of forest debris and agriculture excess that by negligence had gotten out of control. In addition to that, 23% of the fires are caused by criminal activity.

In light of these statistics, it is of extreme importance that an efficient method to cover an area under high risk of ignition and subject to frequent human activity is developed, so that the proper authorities are made aware of the ignitions before they become uncontrollable.

2. Literature Review

The ideal fire detection solution would be one that maintains continuous coverage of an area and is able to identify all sources of ignition. Geostationary satellites provide the first requirement and are already used to monitor environmental phenomena. However, due to the high orbit altitude, approximately 36000 km, the resolution of the obtained data is very low. One example of this is the VAS sensor of the GOES satellite which produces samples of wildfires every three hours with a resolution between 7 and 14 Km on the infrared wavelength [9]. There is the possibility of reducing the satellite's orbit altitude to increase the spatial resolution but there are less availability of such services.

A lower altitude example is the data in gathered in [7], taken from the EOS-MODIS sensor with a resolution of 250m, but is limited to only getting 4 overpasses in a 24 hour period. In addition, data from such measurements can be corrupted by cloud cover [13].

Ground-based detection systems are much cheaper than satellite solutions and are not susceptible to corruption from cloud cover. These provide continuous coverage using visible and subvisible optical sensor, but have very low mobility and are limited to line-of-sight measurements, which can be obstructed by terrain features [1].

This work focuses on Aerial Sensor Networks (ASNs) consisting of fixed-wing Unmmaned Aerial

Vehicles (UAVs) as a means to cover a given area. The problem of patrolling using an ASN can be roughly split into two separate fields of research: area coverage and resource allocation. For a given area to be covered, the area coverage fields deals with ways to optimally covering the allocated region, while the field of resource allocation deals with allocating the different vehicles of the ASN optimally between different subsets of the area to be covered.

For the purpose of this work, optimal allocation of resources means that regions of higher risk are to be monitored more often than areas with a lower risk so that resources are not being wasted at any given time in zones where an ignition is unlikely to start.

Many different measures of risk can be found in [24]. The different measures of risk are mostly based on the economical damage that a wildfire at any given location would cause, weighted by the probability of an ignition in said area.

Both the approaches in [6] and [26] have difficulty assessing the risk caused by human presence, something that is detrimental to any ASN using risk maps generated using these approaches, since the majority of the fires in Portugal is caused by humans (see [16], [19], [8]), as previously mentioned.

With the risk function for a given area, there needs to be a method to guide the agents in the ASN to places with higher risk values more often. The survey [10] describes a number of different strategies for both single and multi-robot area coverage. This problem is related to the so-called "lawnmower problem" which consists on the determination of a path that covers a given area and the "watchman's route problem" which determines the best route to scan the given area. These problems become increasingly difficult as constraints are added to system, such as the presence obstacles, field of view (FOV) restrictions and dynamical constraints. While UAVs are usually not constrained by the presence of obstacles (if their altitude is high enough), they may be subject to dynamical constraints and the onboard sensors may be subject to FOV restrictions. Some of these problems are addressed in [27] and, notably, the authors in [17] follow an approach where point-mass vehicles are routed to areas of higher priority more often.

As stated before, these coverage algorithms can be used in cooperative control with different constraints and objectives. The work in [4] solves the vehicle routing problem optimally with respect to a cost function that minimizes the time it takes to cover a given area, while taking into account the limitations of the vehicles. In [20] and [25] a team of quad-copters is coordinated so as to perform continuous surveillance of a given area while avoiding collisions.

3. Objectives

The objective of this work is to develop a real time trajectory generation algorithm that is capable of allocating resources from a ASN of fixed-wing UAVs dynamically based on the fire hazard risk map on a certain domain, with the goal of maximizing the probability of detecting an ignition. The algorithm can adapt to changes in the risk map so human activity can be taken into consideration. The evaluation of the human risk is not inside the scope of the project, but given the real time data feeds that ASNs are capable of providing, the same algorithm could serve as the basis of such future work.

In order to achieve this goal, the approach used in [17] was chosen as a base. The control law developed in the article does exactly what is necessary: it takes a risk map with very little constraints and guides a network of point-mass agents towards domain zones with high priority in real time. An advantage of this approach is that the risk map can be changed at any time during the mission and the network is able to adapt instantly and keep working as intended. The dynamical systems used in [17] can not be used directly in a real mission, however, because they do not take into account vehicle dynamics. In this work, the control law is adapted in order to take into consideration the dynamics of Fixed-Wing UAVs.

4. Theoretical Background

Given this work's objective of designing an algorithm for uniform coverage provided by an Aerial Sensing Network, it is important to first define what uniform coverage means and how to decide when the coverage is uniform.

In [17], the trajectory is deemed uniform if the dynamical system as a whole possesses ergodicity. Ergodicity is a property of dynamic and stochastic systems that relates the spatial averages of functions to its time averages over a trajectory. That means in a space with a known measure, such as a probability density distribution, the time average of the trajectory will converge to the space measure [21]. In other words, the time spent by an agent of a ergodic dynamical system on a certain space subset is the same as the measure of said subset.

As a result, if the trajectory of the network makes the system ergodic, such a trajectory is deemed uniform and results in an uniform coverage. The primary concern is then how far a system is from being ergodic and how to control the trajectory so the system is ergodic.

5. The metric for uniform coverage

Given a set of N agents for an ASN, let the following distribution C^t be defined:

$$C^t(\mathbf{x}) = \frac{1}{Nt}\int_0^t \sum_{j=1}^{N} \delta(\mathbf{x} - \mathbf{x}_j(\tau))d\tau, \qquad (1)$$

for each $\mathbf{x} \in \mathbb{R}^n$, where $\mathbf{x}_j : [0,t] \to \mathbb{R}^n$ represents the trajectory of the j-th agent for each $j \in \{1, 2, \ldots, N\}$ and $\delta(.)$ is the Dirac delta distribution.

The inner product of the distribution C^t with a bounded generic function f can be written as follows [17]:

$$\langle C^t, f\rangle \ = \frac{1}{Nt}\int_0^t \sum_{j=1}^{N} f(\mathbf{x}_j(\tau))d\tau. \qquad (2)$$

The distribution C^t can be thought of as a probability density distribution because $\langle C^t, 1\rangle \ = 1$. This means C^t can be seen as the probability density distribution function for the position of the agents in the ASN after a time period of t seconds.

Let μ be the measure of a rectangular space with the domain $U \subset \mathbb{R}^n$, with $\mu = 0$ outside of U. For μ to be a measure, it needs to be bounded and non-negative in its domain U. A necessary and sufficient condition to ergodicity is that the time average along a trajectory converges to the average spatial measure [21], so for the system to be ergodic, the convergence of C^t to μ is required. The condition for ergodicity is then:

$$\lim_{t\to\infty} \langle C^t, f\rangle \ = \ \langle \mu, f\rangle$$

for all bounded functions $f : U \to \mathbb{R}$. This is also the definition for weak convergence of the two functions [17].

5.1. Application to a 2D square domain

Given those generalised definitions, let us focus on the case of a 2D square domain, $U = [0, L] \times [0, L]$ for L a positive real number. This is convenient because the domain the ASN needs to cover is a 2D domain.

Let f_k be a Fourier basis functions for the 2D dimensional domain U so that,

$$f_k(\mathbf{x}) \ = \ cos(k_1 x)cos(k_2 y) \qquad (3)$$

for each $\mathbf{x} = (x, y) \in \mathbb{R}^2$, with

$$k_1 = \frac{K_1\pi}{L} \text{ and } k_2 = \frac{K_2\pi}{L}$$

for each $K_1, K_2 = 0, 1, 2, ..., K$, where K is a positive integer, known as the maximum wave number. The subscript k denotes one instance the wave vector $\mathbf{k} = (k_1, k_2)$, for a total of $(1+K)^2$ wave vectors, given that every combination of k_1 and k_2 needs to be considered. The function (3) was used because it satisfies the von Neumann boundary conditions of having a null gradient in the boundaries of domain U.

Using the Fourier basis functions f_k defined in (3), the Fourier coefficients for C^t and μ are given by

$$c_k(t) = \frac{\langle C^t, f_k\rangle}{\langle f_k, f_k\rangle} = \frac{1}{Nt}\frac{\sum_{j=1}^{N}\int_0^t f(\mathbf{x}_j(\tau))d\tau}{\langle f_k, f_k\rangle} \qquad (4)$$

$$\mu_k = \frac{\langle \mu, f_k\rangle}{\langle f_k, f_k\rangle}, \qquad (5)$$

respectively.

To quantify how far the current trajectory is from making the system ergodic, the distance between the two functions C^t and μ is measured using the following metric (cf. [17]):

$$\phi(t) = W_0^t - \mu = \sum_k \Lambda_k s_k(t)^2, \qquad (6)$$

where $s_k(t) = c_k(t) - \mu_k$ and

$$\Lambda_k = \frac{1}{(1 + \mathbf{k}^2)^{\frac{3}{2}}}. \qquad (7)$$

In [18] it is shown that $\phi(t)$ decays to zero if and only if C^t weakly converges to μ. This metric captures the deviation between the time averages and the space averages, and thus how far the system is from being ergodic. It will then be used as the metric for uniform coverage.

6. Fixed-wing airplane models

6.1. Dubin's Vehicle

In this work, it is considered that trajectories of the agents are always in the xOy plane and at a fixed flight altitude, where xOy is part of the NED (North-East-Down) local Inertial frame. As a result, the first system to be considered is that of a Dubin's Vehicle. This system is a described by simple model, which considers that a vehicle moves in a combination of circular arcs and straight lines, with the only control input being the angular velocity of the vehicle's heading angle.

The Dubin's Vehicle motion is interesting because this kind of motion can be associated with the simple coordinated turn model, which directly relates the heading turn ratio with a fixed-wing's roll angle [5]. The equations of motion for the j-th vehicle are the following:

$$\begin{aligned} \dot{\mathbf{x}}_j &= V_g \mathbf{M}(\psi_j) \\ \dot{\psi}_j &= u_j. \end{aligned} \qquad (8)$$

where V_g is a constant scalar value for the vehicle's ground speed, $\mathbf{x}_j$ the vehicle's position, ψ_j is its heading angle, and $\mathbf{M}(\psi_j)$ the projection vector, given by:

$$\mathbf{M}(\psi_j) = \begin{bmatrix} \cos(\psi_j) \\ \sin(\psi_j) \end{bmatrix}. \qquad (9)$$

6.2. Adapted Dubin's Vehicle

For the purpose of having a model with a 2D control input, a model previously studied in [12] was considered.

In this model, instead of tracking the center of mass of the vehicle, a point slightly ahead is considered. The same NED reference frame is used for the inertial frame and a rotating body frame centered on the vehicle's center of mass is considered for the vehicle body, with the linear speed always aligned with the body frame's xx axis so that ${}^B\mathbf{V}_b = [(v_b + \Delta v) \;\; 0]^\top$, where $v_b \in \mathbb{R}$ is a constant value and Δv is an input for the model that belongs to $[-\delta v, \delta v]$ for some positive δv. The position of the tracked point in the body frame is a parameter of the system, $\mathbf{d}_j = [d_1 \;\; d_2]^\top$.

As a result, the tracked dot's position, regarding the j-th agent in the network, $\mathbf{x}_j$ in the inertial frame is calculated using the following expression:

$$\mathbf{x}_j = \mathbf{x}_{cg} + \mathbf{R}(\psi_j)\mathbf{d}_j \tag{10}$$

and its derivative,

$$\dot{\mathbf{x}}_j = \mathbf{R}(\psi_j){}^B\mathbf{V}_b + \dot{\mathbf{R}}(\psi_j)\mathbf{d}_j \tag{11}$$

where $R(\psi_j)$ is the rotation matrix:

$$\mathbf{R}(\psi_j) = \begin{bmatrix} \cos(\psi_j) & -\sin(\psi_j) \\ \sin(\psi_j) & \cos(\psi_j) \end{bmatrix}$$

Assuming a model constraint for the maximum heading rate of vehicle, such that $\dot{\psi}_j \in [-u_{max}, u_{max}]$ and a maximum speed differential of $\Delta v \in [-\delta v, \delta v]$, and with $\mathbf{u}_j = [u_1 \;\; u_2]^\top$ the unitary control input vector, the system (11) can be re-written as follows:

$$\dot{\mathbf{x}}_j = \mathbf{A}(\psi_j)v_b + \mathbf{M}_2(\psi_j)\mathbf{u}_j \tag{12}$$

with $\mathbf{M}_2$ and $\mathbf{A}$ matrices that are functions of the heading angle ψ_j and the different parameters of the system such that,

$$\mathbf{M}_2(\psi_j) = \begin{bmatrix} \delta v \cos(\psi_j) & -u_{max}(d_1 \sin(\psi_j) - d_2 \cos(\psi_j)) \\ \delta v \sin(\psi_j) & u_{max}(d_1 \cos(\psi_j) - d_2 \sin(\psi_j)) \end{bmatrix}$$

$$\mathbf{A}(\psi_j) = \begin{bmatrix} \cos(\psi_j) \\ \sin(\psi_j) \end{bmatrix}$$

for each $\psi_j \in \mathbb{R}$.

In this model, the determinant of matrix $\mathbf{M}_2(\psi_j)$ is given by $\det(\mathbf{M}_2(\psi_j)) = \delta v \cdot d_1 \cdot u_{max}$ and it is different than zero for every heading value as long as long as δv, u_{max} nor d_1 are not zero themselves, making it so there are never problems with matrix inversion.

Another noteworthy fact is that both inputs are directly available in the first derivative of the UAV positions directly, which is very important in the next section.

7. Feedback Control Law

Calculating the optimal control law is done by solving the optimal control problem over a finite time horizon $[t, t + \Delta t]$ when Δt tends to zero. This approach was employed in [17] and is explained in [14]. In order to do this, it is more convenient to express the quantities from Section 5 without the time factor and the number of agents in the denominator, by multiplying the quantities by Nt as follows:

$$\begin{aligned} C_k(t) &= \frac{\sum_{j=1}^{N} \int_0^t f(\mathbf{x}_j(\tau))d\tau}{\langle f_k, f_k \rangle} = Ntc_k(t) \\ U_k(t) &= Nt\mu_k \\ S_k(t) &= C_k(t) - U_k(t) = Nts_k(t) \\ \Phi(t) &= \sum_k \Lambda_k S_k(t)^2 = N^2t^2\phi(t). \end{aligned}$$

To solve the optimal control problem, an appropriate cost function must be picked and the Hamiltonian equation formulated. For this purpose, the chosen cost function to minimise is the derivative of the metric for uniform coverage $\Phi(t + \Delta t)$, namely $\dot{\Phi}(t + \Delta t)$, which means that the goal is to make the next position of the agent so that the metric for uniform coverage decays as much as possible, leading to the lowest possible value of the metric for uniform coverage. This derivative is as follows,

$$\dot{\Phi}(t + \Delta t) = \sum_k \Lambda_k S_k(t) \frac{dS_k(t)}{dt}. \tag{13}$$

with

$$\frac{dS_k(t)}{dt} = \frac{\sum_{j=1}^{N} f_k(\mathbf{x}_j(t))}{\langle f_k, f_k \rangle} - N\mu_k, \tag{14}$$

where $\nabla f_k(.)$ is the gradient vector of the Fourier basis function.

For all the models, the chosen cost function to minimize is:

$$J(t, \Delta t) = \dot{\Phi}(t + \Delta t) \tag{15}$$

In this specific case, without a Lagrangian function in the cost, the necessary conditions for optimality of the control problem in the interval $[t_0, t_f]$ are explained in [14] and are as follows:

$$\dot{\mathbf{x}}^*(t) = \frac{\partial \mathcal{H}}{\partial \lambda}(\mathbf{x}^*(t), \mathbf{u}^*(t), \lambda^*(t), t) \tag{16}$$

$$\dot{\lambda}^*(t) = -\frac{\partial \mathcal{H}}{\partial \mathbf{x}}(\mathbf{x}^*(t), \mathbf{u}^*(t), \lambda^*(t), t) \tag{17}$$

$$\mathcal{H}(\mathbf{x}^*(t), \mathbf{u}^*(t), \lambda^*(t), t) \leq \mathcal{H}(\mathbf{x}^*(t), \mathbf{u}(t), \lambda^*(t), t), \tag{18}$$

where $\mathbf{x}(t)$ and $\mathbf{u}(t)$ are generic system states and control inputs, $\lambda(t)$ are the costates for the minimization and $\mathcal{H}(\mathbf{x}(t), u(t), \lambda(t), t)$ is the Hamiltonian function. This, of course, for every $t \in [t_0, t_f]$ and every admissible control input. The * superscript means optimality, such as the optimal input $\mathbf{u}^*$.

7.1. Dubin's vehicle control law

Let us then consider the extended system for the Dubin's Vehicle, adding the equations for the auxiliary states $S_k(t)$ and $O_k(t) = \dot{S}_k(t)$:

$$\begin{aligned} \dot{\mathbf{x}}_j &= V_a \mathbf{M}(\psi_j) \\ \dot{\psi}_j &= u_j \\ \dot{S}_k(t) &= O_k(t) \\ \dot{O}_k(t) &= \sum_{j=1}^{N} \frac{\nabla f_k(\mathbf{x}_j(t))}{\langle f_k, f_k \rangle} \cdot \dot{\mathbf{x}}_j(t) \end{aligned} \tag{19}$$

Now, let the costates be ${}^j\lambda_1(\tau) \in \mathbb{R}^2$ and ${}^j\lambda_2(\tau), {}^k\lambda_3(\tau), {}^k\lambda_4(\tau) \in \mathbb{R}$ for all N agents and for all k wave number vectors.

The Hamiltonian is defined for each $\tau \in [t, t+\Delta t]$ and written as follows:

$$\begin{aligned} &\mathcal{H}(x_j, \psi_j, S_k, O_k, u_j, {}^j\lambda_1, {}^j\lambda_2, {}^k\lambda_3, {}^k\lambda_4, \tau) = \\ &= V_a \sum_{j=1}^{N} {}^j\lambda_1 \cdot \mathbf{M}(\psi_j) + \sum_{j=1}^{N} {}^j\lambda_2 u_j + \sum_k {}^k\lambda_3 O_k \\ &\quad + V_a \sum_k {}^k\lambda_4 \frac{\sum_{j=1}^{N} \nabla f_k(\mathbf{x}_j)}{\langle f_k, f_k \rangle} \cdot \mathbf{M}(\psi_j) \end{aligned} \tag{20}$$

where the time dependencies on the states were omitted for brevity.

The control input u_j in this model is bounded, its upper and lower values being u_{max} and $-u_{max}$, respectively. As such, the optimization of the optimal control problem is done by minimizing the Hamiltonian, seen in (18). The control law is then given by:

$$u_j^*(\tau) = \underset{||u_j(\tau)|| \leq u_{max}}{\arg\min} \; \mathcal{H}(.) \tag{21}$$

for each $\tau \in [t, t+\Delta t]$. The solution to that equation is trivial, as only the second term of the Hamiltonian contains the control input. As such, the optimal control law can be written as follows:

$$u_j^*(\tau) = -\frac{{}^j\lambda_2(\tau)}{||{}^j\lambda_2(\tau)||} u_{max}. \tag{22}$$

for each $\tau \in [t, t + \Delta t]$.

Defining the auxiliary variable $\beta_j(t)$ as

$$\beta_j(t) = V_a \sum_k \Lambda_k S_k(t) \frac{\sum_{j=1}^{N} \nabla f_k(\mathbf{x}_j(t))}{\langle f_k, f_k \rangle} \cdot \frac{\partial \mathbf{M}}{\partial \psi_j}, \tag{23}$$

the final control law for the Dubin's Vehicle is the following expression,

$$u_j^*(t) = -u_{max} \text{sign}(\beta_j(t)) \tag{24}$$

7.2. Adapted Dubin's vehicle control law

Let us then consider the extended system for the Adapted Dubin's Vehicle, adding equations for the auxiliary states $S_k(y)$ and $O_k(t) = \dot{S}_k(t)$:

$$\begin{aligned} \dot{\mathbf{x}}_j(t) &= \mathbf{A}(\psi_j) v_b + \mathbf{M}_2(\psi_j) \mathbf{u}_j \\ \dot{S}_k(t) &= O_k(t) \\ \dot{O}_k(t) &= \sum_{j=1}^{N} \frac{\nabla f_k(\mathbf{x}_j(t))}{\langle f_k, f_k \rangle} \cdot \dot{\mathbf{x}}_j(t) \end{aligned} \tag{25}$$

With analogous costates ${}^j\lambda_1(\tau) \in \mathbb{R}^n$ and ${}^k\lambda_2(\tau), {}^k\lambda_3(\tau) \in \mathbb{R}$ for all N agents and K wave vector harmonics, the Hamiltonian equation can be written as follows,

$$\begin{aligned} &\mathcal{H}(x_j, S_k, O_k, u_j, {}^j\lambda_1, {}^k\lambda_3, {}^k\lambda_4, \tau) = \\ &\sum_{j=1}^{N} {}^j\lambda_1 \cdot [\mathbf{A} v_b] + \sum_{j=1}^{N} {}^j\lambda_1 \cdot [\mathbf{M}_2(\psi_j) \mathbf{u}_j] + \sum_k {}^k\lambda_2 O_k \\ &\quad + \sum_k {}^k\lambda_3 \frac{\sum_{j=1}^{N} \nabla f_k(\mathbf{x}_j)}{\langle f_k, f_k \rangle} \cdot [\mathbf{M}_2(\psi_j) \mathbf{u}_j + \mathbf{A} v_b] \end{aligned} \tag{26}$$

for each $\tau \in [t, t+\Delta t]$, where the time dependencies were again omitted for brevity.

The control input is defined in this model as a vector with maximum norm equal to one, with the amplitudes of velocity and heading turn rate dictated by parameters and as such not included in the input. As a result, the boundaries for the input are $\mathbf{u}_j(t) \leq 1$. The optimal control input is then

$$\mathbf{u}_j^*(\tau) = \underset{||u_j(\tau)|| \leq 1}{\arg\min} \; \mathcal{H}(.) \tag{27}$$

For a cleaner expression, let's define the auxiliary variable $\beta_j(t)$ so that

$$\beta_j(t) = \mathbf{M}_2^T(\psi_j(t)) \sum_k \Lambda_k S_k(t) \frac{\sum_{j=1}^{N} \nabla f_k(\mathbf{x}_j(t))}{\langle f_k, f_k \rangle}.$$

Given the bounded nature of the input, the optimal control law can be written as

$$\mathbf{u}_j^*(t) = -\frac{\beta_j(t)}{||\beta_j(t)||} \tag{28}$$

8. Target probability density distribution

8.1. Fire Hazard Risk

The concept of uniform coverage based control laws obtained in Section 7 is the convergence of the time average along a trajectory into the desired spatial

measure. The spatial measure is then one of the inputs of the algorithm.

As previously mentioned in Section 5, the only restriction applied to this measure is that it needs to be bounded, without infinite values in the space domain that needs to be surveilled.

For the purpose of this work, it is convenient to think of this measure as something that relates to fire hazard risk. A measure that would make sense is the Fire Hazard Risk Index, a value calculated daily by IPMA. According to the methodology document publicly available [11], this value is a number from one to five, encompassing the different risk levels from reduced to maximum, calculated using various data such as weather prediction and the amount of fuel on the ground.

8.2. Designing the target probability density distribution

Considering that further in the work there will be a probability analysis, it is convenient that the measure for the Fire Hazard Risk is expressed as a probability density distribution with a volume of one in the entire domain.

Let $U = [0, L] \times [0, L] \subset \mathbb{R}^2$ be the square target domain for surveillance and $\mu : \mathbb{R}^2 \to \mathbb{R}$ the target probability density distribution. Using an auxiliary function, $risk : \mathbb{R}^2 \to \mathbb{R}$ which assigns a relative risk number to every point in the domain, we can have the target probability density distribution defined as

$$\mu(x, y) = \frac{risk(x, y)}{\iint_U risk(X, Y) dX dY} \tag{29}$$

for every $(x, y) \in U$. The function is zero for every (x, y) outside of the domain U.

For simulation purposes, the domain picked is a $2000m \times 2000m$ domain with a cell resolution of $100m \times 100m$, but in order to avoid symmetry issues caused by the Fourier basis function (3), the domain is extended with values equal to zero. The graphical representation is shown in Figure 8.2.

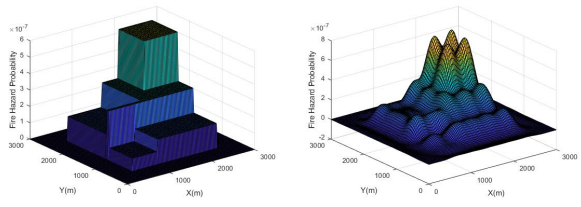

(a) Fire Hazard probability (b) Fourier Transform of the Fire Hazard probability

Figure 1: Fire Hazard probability function and its Fourier approximation with $K = 15$.

9. Simulink Simulations

For the Simulink simulations, we considered an ASN composed of 3 UAVs with a maximum heading rate of $u_{max} = 0.5rad/s$ and a constant vehicle speed of $Va = 30m/s$.. The simulation was run for a period of $T = 3600s$, i.e., one hour. The equations were solved using the *ode4* solver with a step time of $0.1s$.

10. Dubin's Vehicle Model Simulation

The metric for uniformity obtained in the simulation is showcased in Figure 4, and it shows the expected decay. The metric is not monotonous, which wouldn't be possible, but the control law guarantees that should there be an increase, it is the smallest possible. Overall, the trend is that the metric is converging to zero.

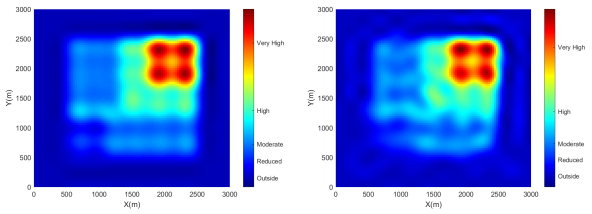

(a) Heatmap of the desired probability density distribution (b) Heatmap of the obtained probability density distribution

Figure 2: Visualization of the desired probability density distribution's and the obtained probability density distribution's Heatmap.

An easier visualization of the results is shown in Figure 10, showing the heatmap comparison between the desired distribution and the obtain probability density distribution. The heatmaps are very similar, a result that suggests that the adaptation was successful, as ultimately, the agents were distributed correctly.

There is an issue with the control input of this model, stemming from (21). The control input for this model is an erratic discrete signal that bounces between the minimum and maximum values.

11. Adapted Dubin's Vehicle Model

For the Adapted Dubin's Vehicle model, the parameters chosen were $d_2 = 0m$, $d_1 = 0.5m$ and $\delta v = 5m/s$.

The metric for uniformity is plotted in Figure 4, in blue, and shows a decrease in average value over time, suggesting it would successfully converge to zero for an infinite mission.

The heatmap probability density distribution obtained in this simulation is shown in Figure 11, and has a shape that is very similar to the reference distribution. This model has no issues with the control input, given that the optimal control law (28) is not

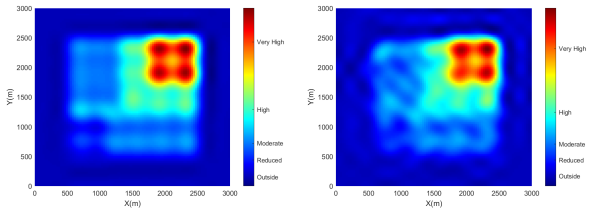

(a) Heatmap of the desired probability density distribution

(b) Heatmap of the obtained probability density distribution.

Figure 3: Visualization of the desired probability density distribution's and the obtained probability density distribution's Heatmap on the Adapted Dubin's Vehicle Model.

discrete, with the control input being any value in the unitary sphere.

12. Model performance comparison

Since both the previous models had the same initial condition, same domain, and same risk function, it is possible to overlap the metric for uniform coverage graphs.

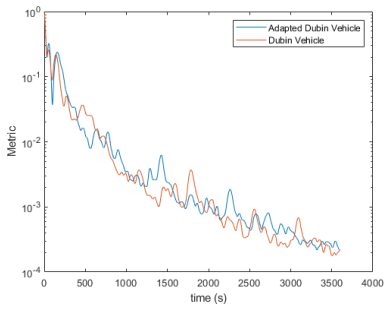

Figure 4: Comparison between the metric for uniform coverages of the Dubin's Vehicle and the Adapted Dubin's Vehicle.

In Figure 4, the two metrics are overlapped and look very similar. The Dubin's Vehicle model has a slightly lower average value, but the results could have easily been passed as eachother's, as they have no noticeable differences. This suggests that the Adapted Dubin's Vehicle model would be a more sensible choice for implementation in real life as there is no issue with the control input being discrete and erratic.

13. ROS Implementation

A ROS implementation of the Dubin's Vehicle was done using a generic fixed-wing UAV with VTOL capabilities in Gazebo. The UAV was controlled using the PX4 stack in *offboard* mode, sending waypoints that were generated with the state equations for the model.

To calculate the optimal control law, the control station receives GPS data from the aircraft. The position values and the ground speed values are needed. The ground speed is used to calculate the heading as follow:

$$\psi = atan2(V_y, V_x)$$

where V_x and V_y are the linear speed components in the inertial frame.

Due to hardware limitations, only one aircraft was considered for this simulation. Furthermore, due to technical constraints in the PX4 controller stack, only the Dubin's Vehicle Model was able to be implemented without deeply delving into the PX4 source code, which is outside of the scope of this work.

The aircraft speed was set to $25m/s$ instead of the previous simulation's $30m/s$ due to vehicle limitations. The maximum heading turn rate was set to $u_{max} = 0.5rad/s$. The simulation time was extended to around 6000 seconds from the previous 3600 seconds because of the decrease in speed and number of aircrafts. The communications between the vehicle and the control station took place with a frequency of 10Hz.

14. Results of the ROS simulation

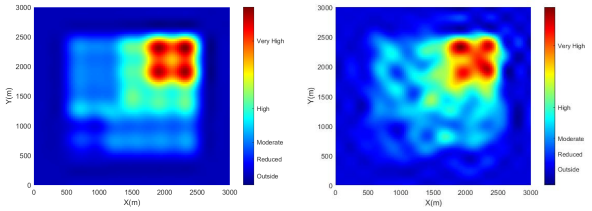

(a) Heatmap of the desired probability distribution

(b) Heatmap of the obtained probability distribution.

Figure 5: Visualization of the desired probability distribution's and the obtained probability distribution's Heatmap on ROS/Gazebo simulation.

The heatmap for the vehicle's position probability distribution is showcased in Figure 14, and it shows that there are clear differences between the obtained result and the desired output. This is most likely due to the difficulty the PX4 controller has in following the desired waypoints due to the discrete and erratic nature of the control input. However, due to the fact that only one aircraft was considered and the conditions were not ideal (i.e. inefficient control method for the model used, and the use of the Dubin's Vehicle model), the result shows the overall shape of the distribution was still achieved, and that higher risk areas were covered for longer than lower risk areas.

15. Ignition Definition

In order to estimate of the probability of detection of an ignition during a surveillance mission, it is

important to define what is to be considered an ignition.

For the purpose of this work, an ignition is to be the precursor to an uncontrollable fire, a small flame that might be contained easily and in a timely manner. With the most common fire causes mentioned in Section 1, this can be associated with a Crawling or Surface fire. A Crawling or Surface fire is a fire caused by the burning of ground level vegetation and other fuels such as grass, trash debris, and pieces of wood from surrounding trees. These fires burn with a surface temperature of around 400ºC to 500ºC [3].

In [2], it is concluded that the type of IR sensor more suited to detect fire is a MWIR due to the radiation at fire temperatures peaking at a wavelength between $3\mu m$ and $3\mu m$, which is inside the MWIR sensing range.

16. Probability of Detection

Let a UAV position (x_v, y_v) be a point in the coverage domain U. With the last moment of the simulation taken into consideration, the probability of one UAV in the network being in (x_v, y_v) is $P_v(x_v, y_v)$, defined as

$$P_v(x_v, y_v) = C^{t=3600}. \tag{30}$$

The probability density distribution of an ignition is the target distribution function of the algorithm, μ. As such, let (x_i, y_i) be a point in the coverage domain U. The probability of an ignition happening in (x_i, y_i) is $P_i(x_i, y_i)$, defined as

$$P_i(x_i, y_i) = \mu(x_i, y_i). \tag{31}$$

16.1. Sensor Model

The model used for this part was proposed in [15] and takes advantage of the fact that electromagnetic radiation propagates spherically in a vacuum and in a free medium such as air. The result of this is that the power dissipation is proportional to the inverse of the distance travelled squared. As such, the noisy measurement obtained by the IR sensor can be modelled by the following equation,

$$P_r(x_v, y_v, x_i, y_i) = \frac{P_{0i}}{4\pi R(x_v, y_v, x_i, y_i)^2} + n_i \tag{32}$$

where he power P_{0i} is defined by the Stefan-Boltzmann law, which is a valid way to model a fire [23], he parameter n_i is a random variable following a Gaussian distribution and $R(x_v, y_v, x_i, y_i)$ is the distance between the ignition point and the sensor position, which is the vehicle position, given by

$$R(x_v, y_v, x_i, y_i) = ||(x_v, y_v, h) - (x_i, y_i, 0)|| \tag{33}$$

where h is the flight altitude of the vehicle, a constant parameter over the surveillance mission.

The proposed model for the probability of detection is based on whether the power received by the sensor is higher than a certain threshold. Consequently, let $P_{sens}(x_v, y_v, x_i, y_i)$ be the probability of the sensor detection,

$$P_{sens}(x_v, y_v, x_i, y_i) = \{P_r(x_v, y_v, x_i, y_i) > c\}. \tag{34}$$

The important variables to determine for this model are then the standard deviation of the white noise added to the received power and the threshold at which a detection is deemed to have failed.

To obtain the value of c, a distance from the ignition at which the sensor has a 50% chance of detection needed to be chosen. The distance chosen for the analysis is $5000m$. The standard deviation was picked so that there is a decrease of 90% of the probability between 4500m and 5500m.

Not only are the sensors limited by distance, they are also limited by their field of view. To take in consideration the FOV of the sensor, it will be assumed that the sensor is always pointing straight down from the aircraft and has a conic field of view. The radius of the cone on the ground can then be written as follows,

$$r = h \arctan(\frac{\gamma}{2}),$$

where h is the flight altitude and γ is the angle of the cone of view. This angle can range between different values even in the same sensor, but as it increases the resolution of the obtained image also decreases due to more area being covered with the same amount of pixels. The value used throughout this section is $\gamma = 24^{\text{o}}$.

Ultimately, the sensor model to be used it P_s, defined as follows,

$$P_s(x_i, y_i, x_v, y_v) = \begin{cases} P_{sens}(x_i, y_i, x_v, y_v) & \text{if } R \leq r \\ 0 & \text{otherwise} \end{cases}. \tag{35}$$

16.2. Probability function

With a well defined sensor model, vehicle position probability density distribution and ignition probability density distribution, the overall probability of one UAV in the network detecting an ignition can be the integral of the product of those three,

$$P_d = \iint_U \iint_U P_s(x_v, y_v, x_i, y_i) P_i(x_i, y_i) P_v(x_v, y_v). \tag{36}$$

The detection of an ignition is an independent event for each aircraft in the network, so the joint probability of detection is given as

$$P_{joint} = 1 - \prod_{i=1}^{N}(1 - P_d). \tag{37}$$

17. Parametric Study

In order to maximize the joint probability of detection, the flight altitude was varied between $h = 500m$ and $h = 5500m$. The probabilities obtained are showcased in Figure 6.

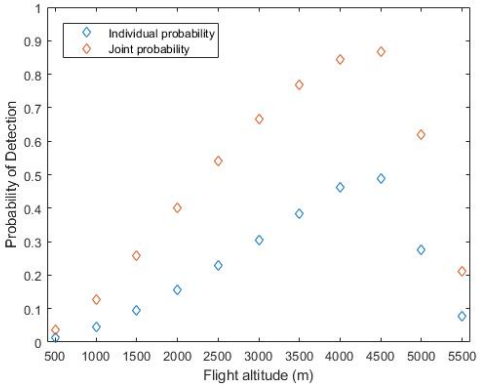

Figure 6: Probability of detecting an ignition in function of the altitude.

The figure clearly shows that there is an optimal altitude, with a sharp decrease afterwards and a steady climb up until that point. The steady climb up to the optimal altitude is the result of the FOV restrictions, when the distance between the sensor and ignition is still low enough that there is no drop in performance in that front. As the altitude increases, more area is covered at the same time and with good performance, leading to the increase as altitude goes up. However, after the $h = 4500m$ mark, the performance drops sharply, which is the result of the threshold value chosen for the sensor model, which dictates a performance drop after a distance of $5000m$ from the ignition. At this point, increasing the altitude only means the performance of the sensor drops even further, which is not offset by the increased area covered.

A better sensor would mean this threshold could be increased, or that the FOV angle could be increased without any significant drop in resolution, which would shift the curves up and increase the probability of detection. Additionally, adding more agents would significantly increase the joint probability of detection, as shown in (37).

18. Conclusion

Overall, the objectives outlined in Section 3 were all properly accomplished throughout this work. The theoretical basis for the algorithm was established in Section 4, with all the functions defined for understanding how to say if the trajectories of the system can be considered uniform. In light of the movement restrictions of a fixed-wing UAV, two different movement models were introduced in that are easily associated with the coordinated turn movement of an aircraft. By the end of Section , the optimal feedback control laws for both models were obtained.

In Section 8, the Fire Hazard Risk function was defined in order to run Matlab/Simulink simulations for both models. The results of the simulation for the Dubin's Vechicle Model in Section 10 show that the metric for uniform coverage converges to nearly zero, and the heatmaps of the probability distribution function of the UAV position closely resemble the desired heatmap.

The results of the simulation for the Adapted Dubin's Vehicle Model in Section 11 show that the performance is equivalent to the performance in of the Dubin's Vehicle Model but without the issue of the discrete control input.

The real time component of the trajectory generation proved to be possible to implement within the limitations of a real life environment by running an unoptimised ROS simulation using the Gazebo physics simulator and a PX4 vehicle model for simulation in Section 13.

In Section 15, the concept of ignition was defined in order for a probabilistic model for the ignition detection probability to be proposed. A sensor model for a Infra-Red sensor was proposed and is the basis for the probabilistic model. The parametric study shows there is a clear optimal altitude which varies depending on the sensor used.

18.1. Future Work

Interesting future work that could be done is the integration of the sensor model into the optimal control law, as it is clearly a bottleneck for the probability of detection, as well as scaling the algorithm for 3D trajectories and adding the flight altitude to the optimal control law.

There might also be the case that using the Fire Hazard Risk function as the target measure does not maximize the probability of detection, so the optimization problem could be further studied by, for example, applying genetic algorithms to (36).

References

[1] A. Alkhatib. A review on forest fire detection techniques. *International Journal of Distributed Sensor Networks*, 2014, 03 2013.

[2] R. S. Allison, J. M. Johnston, G. Craig, and S. Jennings. Airborne optical and thermal remote sensing for wildfire detection and monitoring. *Sensors*, 16(8), 2016.

[3] W. J. B. S. J. P. M. E. A. Andrew C. Scott, David M. J. S. Bowman. *Fire on Earth: An Introduction*. Wiley-Blackwell, 2014.

[4] G. Avellar, G. Pereira, L. Pimenta, and P. Iscold. Multi-uav routing for area coverage and remote sensing with minimum time. *Sensors*, 15:27783–27803, 11 2015.

[5] R. W. Beard and T. W. McLain. *Small Unmanned Aircraft: Theory and Practice*. Princeton University Press, 2012.

[6] R. F. B. F. M. F. Catry, F. X. Modeling and mapping wildfire ignition risk in portugal. *International Journal of Wildland Fire.*, 18:921–931, 2009. https://doi.org/10.1071/WF07123.

[7] D. de Gestão de Áreas Públicas e de Protecção Florestal. 10º relatório provisório de incêndios florestais, 2017.

[8] D. de Gestão de Áreas Públicas e de Protecção Florestal. 6º relatório provisório de incêndios florestais, 2021.

[9] B. E and A. C. *Introduction to Satellite Remote Sensing*. Elsevier, 2017.

[10] E. Galceran and M. Carreras. A survey on coverage path planning for robotics. *Robotics and Autonomous Systems*, 61(12):1258–1276, 2013.

[11] IPMA. Cálculo do Índice de risco de incêndio rural risco conjuntural e meteorológico – rcm. Technical report, Instituto Português do Mar e da Atmosfera, I.P., 2020.

[12] R. W. B. J. R. T. Lawton and B. J. Young. A decentralized approach to formation maneuvers. *IEEE Transactions on Robotics*, 19(6):933–941, 2003.

[13] Y. J. Kaufman, C. O. Justice, L. P. Flynn, J. D. Kendall, E. M. Prins, L. Giglio, D. E. Ward, W. P. Menzel, and A. W. Setzer. Potential global fire monitoring from eos-modis. *Journal of Geophysical Research: Atmospheres*, 103(D24):32215–32238, 1998.

[14] D. E. Kirk. *Optimal control theory: an introduction*. Dover Publications, 2004.

[15] W. Li and C. Cassandras. Distributed cooperative coverage control of sensor networks. In *Proceedings of the 44th IEEE Conference on Decision and Control*, pages 2542–2547, 2005.

[16] L. Lourenço and M. Mira. Grandes incêndios florestais de 17 de junho de 2017 em portugal e exemplos da determinação das respetivas causas. *Territorium*, 26(II):49–60, 2019.

[17] G. Mathew and I. Mezi. Metrics for ergodicity and design of ergodic dynamics for multi-agent systems. *Physica D: Nonlinear Phenomena*, 240(4-5):432–442, Feb. 2011. 10.1016/j.physd.2010.10.010.

[18] G. Mathew, I. Mezi, and L. Petzold. A multiscale measure for mixing. *Physica D: Nonlinear Phenomena*, 211(1-2):23–46, Nov. 2005. 10.1016/j.physd.2005.07.017.

[19] A. C. Meira Castro, A. Nunes, A. Sousa, and L. Lourenço. Mapping the causes of forest fires in portugal by clustering analysis. *Geosciences*, 10(2), 2020.

[20] N. Michael, E. Stump, and K. Mohta. Persistent surveillance with a team of mavs. In *2011 IEEE/RSJ International Conference on Intelligent Robots and Systems*, pages 2708–2714, 2011.

[21] K. E. Petersen. *Ergodic theory*. Cambridge University Press, 1989.

[22] L. Pinto. Pedrógão grande: Governo estima prejuízos de 500 milhões de euros, 2017. Last Visited: 10/14/2021.

[23] J.-L. Rossi, K. Chetehouna, A. Collin, B. Moretti, and J.-H. Balbi. Simplified flame models and prediction of the thermal radiation emitted by a flame front in an outdoor fire. *Combustion Science and Technology*, 182(10):1457–1477, 2010.

[24] D. Thomas, D. Butry, S. Gilbert, D. Webb, and J. Fung. The costs and losses of wildfires: a literature survey. Technical report, nov 2017.

[25] P. Tokekar, A. Budhiraja, and V. Kumar. Algorithms for visibility-based monitoring with robot teams. 12 2016.

[26] J. C. Verde and J. L. Zêzere. Assessment and validation of wildfire susceptibility and hazard in portugal. *Natural Hazards and Earth System Sciences*, 10(3):485–497, 2010.

[27] A. Xu, C. Viriyasuthee, and I. Rekleitis. Optimal complete terrain coverage using an unmanned aerial vehicle. In *2011 IEEE International Conference on Robotics and Automation*, pages 2513–2519, 2011.